Ceramics International 47 (2021) 15639–15647

Contents lists available at ScienceDirect

Ceramics International

journal homepage: www.elsevier.com/locate/ceramint

Novel and efficient hybrid supercapacitor of chemically synthesized quaternary 3D nanoflower-like $NiCuCo_2S_4$ electrode

Surendra K. Shinde [a], Hemraj M. Yadav [b], Gajanan S. Ghodake [a], Ajay D. Jagadale [c], Monali B. Jalak [d], Dae-Young Kim [a,*]

[a] Department of Biological and Environmental Science, College of Life Science and Biotechnology, Dongguk University, 32 Dongguk-ro, Biomedical Campus, Ilsandong-gu, Siksa-dong, 10326, Goyang-si, Gyeonggi-do, South Korea
[b] Department of Energy and Materials Engineering, Dongguk University, Seoul, 04620, South Korea
[c] Center for Energy Storage and Conversion, School of Electrical and Electronics Engineering, SASTRA Deemed University, Thanjavur, 613401, Tamilnadu, India
[d] Department of Physics, Shivaji University, Kolhapur, 416004, M.S, India

ARTICLE INFO

Keywords:
Novel quaternary electrode
$NiCuCo_2S_4$
Nanoflowers
Transition metal sulfide (TMS)
Supercapacitive properties

ABSTRACT

In this work, we employed a simple and cost-effective chemical route to obtain a highly stable and efficient quaternary mesoporous 3D nanoflower-like $NiCuCo_2S_4$ nanocomposite for supercapacitor applications. The $NiCuCo_2S_4$ composite exhibited a mixture of $NiCo_2S_4$ and $CuCo_2S_4$ phases, confirming the formation a quaternary $NiCuCo_2S_4$ thin film. A surface morphological analysis revealed the unique nanoflower-like nanostructure of the annealed composite. The electrochemical analysis of the $NiCuCo_2S_4$ electrode demonstrated a high specific capacity (Cs) of 414 mAh g^{-1} at a lower scan rate of 10 mV s^{-1} and a superior cycling stability up to 3000 cycles. A solid-state hybrid supercapacitor (SHS) was also constructed by the $NiCuCo_2S_4$ and AC powder as positive and negative electrodes, respectively. The $NiCuCo_2S_4$//AC hybrid cell produced a high Cs, energy density, and power density of 159 F g^{-1}, 35.19 Wh kg^{-1}, and 0.66 kW kg^{-1}, respectively at a current density of 10 mA with good cycling stability. The results demonstrated that the fabrication process is effective for the development of a novel quaternary transition metal sulfide (TMS) electrode.

1. Introduction

The expansion of a high-energy storage system has fascinated significant consideration due to the rising demand for efficient renewable energy sources. The capable energy storage systems such as supercapacitors (Sc) offer a high power density, energy density, cycling stability, lower resistance, and greater safety compared to batteries [1,2]. Electrochemical supercapacitors store energy either through ion adsorption (electrochemical double-layer capacitors, EDLCs) or fast, reversible, multi-electron surface redox reactions (pseudocapacitors). Highly reversible redox reactions are responsible for the high specific capacitance of pseudocapacitor devices [3–5]. Physicochemical properties of the selected materials strongly affect the performance of supercapacitor devices. For instance, the electrochemical performance can degrade during the cycling due to change in the morphology of selected materials. Therefore, it is important to improve the morphological stability of supercapacitive electrode materials to maximize their cycle life [6]. Materials with hierarchical pores and tabular or layered structures are well-known to increase the charge transport, ion diffusion, power density, and the cycling stability [1,7]. In addition to structural design, the electrode composition also have a crucial role in the performance of electroactive materials [8]. The electrochemical performance can be tuned by optimizing the ratio of metal ions.

Several nanomaterials with desirable properties fabricated from carbonaceous materials and metal oxides have been employed in supercapacitor applications. In particular, metal chalcogenides exhibit excellent physiochemical properties that are suitable for supercapacitor applications. Ni, Co, and Cu-based materials have attracted significant attention in various fields, the oxides and sulfides of these metals have been proven to be useful for electrochemical energy storage applications [9]. These metals are an important strategic resources which are mostly suitable in electrochemical energy storage systems, catalysis, and other fields due to their unusual structural, optical, and electronic properties [10]. Ni, Co, and Cu-based battery materials in aqueous and alkaline electrolytes have been reported to facilitate fast Faradaic reactions on or near their surface, thus offering both high energy storage and power

* Corresponding author.
E-mail address: sbpkim@dongguk.edu (D.-Y. Kim).

https://doi.org/10.1016/j.ceramint.2021.02.134
Received 12 January 2021; Received in revised form 7 February 2021; Accepted 15 February 2021
Available online 18 February 2021

performance [8]. The redox peaks in cyclic voltammograms (CVs) and the plateau in galvanostatic charge–discharge (GCD) curves are features for battery materials that differ from those of pseudocapacitive materials, which exhibit rectangular CVs and linear GCD curves [11,12].

The preparation of metal sulfides (MS) has been achieved using many techniques, such as chemical bath deposition, hydrothermal, co-precipitation, and successive ionic layer adsorption and reaction. Among the many deposition techniques that have already been employed, the co-precipitation is a particularly attractive and versatile approach because of its easiness, low price, and easily controllable deposition parameters. TMS have been previously used for energy storage and conversion applications such as supercapacitor, solar cell, battery, hydrogen (HER) and oxygen (OER) evolution reaction, however, a less attention has been paid to the use of quaternary sulfide electrodes in electrochemical supercapacitor [5,13–17]. Recently, Xu et al. [18] synthesized a Ni–Co–Cu composite using chemical etching followed by hydrothermal. They found that the capacitance was 1.3 times higher after 1000 cycles. In addition, Wu et al. [19] prepared Ni, Cu, and Co-based mixed-metal oxyphosphide nanowire arrays anode for a lithium storage using hydrothermal. Gu et al. [20] fabricated asymmetric supercapacitor (ASC) device, consisting of Ni and Zn co-substituted Co carbonate hydroxide on Ni foam which displayed an energy density of 29.6 Wh kg^{-1} at a power density of 375 W kg^{-1}. Similarly, Ahsan et al. [21] fabricated a ASC of $ZnNiCo_2O_4$ nanowires by the hierarchical growth of $ZnNiCo_2O_4$ nanoparticles, and multi-walled carbon nanotubes. Their ASC exhibited an energy density of 37.89 Wh kg^{-1} and an excellent capacitance retention for the number of cycles. The microstructural and magnetic properties of Cu–Co–Ni ternary alloys prepared using electrodeposition was studied by Karpuz et al. [22]. Similarly, the electrodeposition of CoCu, NiCo, and NiCoCu in a slightly acidic citrate electrolyte was investigated by Ignatova et al. [23], while Jafarian et al. [24] studied the electrocatalytic activity of hydrazine oxidation using a CuCoNi based ternary materials on graphite and found that the prepared NiCoCu based ternary material are useful for the improvements in the oxidation of hydrazine. Recently, various Ni–Co–Cu–Zn based nanostructures have been synthesized and employed as electrocatalysts. However, to the best of our knowledge, the preparation of $NiCuCo_2S_4$ via chemical co-precipitation has not been reported for solid state hybrid supercapacitor (SHS) applications. Herein, we summarized previously reported synthesis methods and applications of $NiCuCo_2S_4$ by algorithmically (as shown in the Algorithm chart 1) [25–30]. This algorithm clearly shows that there are very few reports available on supercapacitors and solid state hybrid supercapacitor evaluation.

Herein, we designed a new fabrication strategy to produce a quaternary $NiCuCo_2S_4$ electrode on Ni foam by screen-printing method. The structural and morphological results confirmed the optimistic consequence on the nanostructure and porosity of the fabricated electrode. The optimized $NiCuCo_2S_4$ electrode presented a higher Cs of 414 mAh g^{-1} at 10 mV s^{-1} and better cycling stability. A solid-state $NiCuCo_2S_4$// AC hybrid device have a higher energy density of 35.19 Wh kg^{-1} at a power density of 0.66 kW kg^{-1}, with an excellent energy density of 12.21 Wh kg^{-1} at a power density of 20 kW kg^{-1}. Based on the long-term durability results, it can be concluded that the solid-state $NiCuCo_2S_4$// AC hybrid device has higher electrical storage capacity. This also proves that the quaternary $NiCuCo_2S_4$ electrode is more efficient and stable for use in electrochemical energy storage and conversion applications.

Algorithm chart 1. Schematic of the ternary transition metal sulfides/oxides composites and their preparation methods.

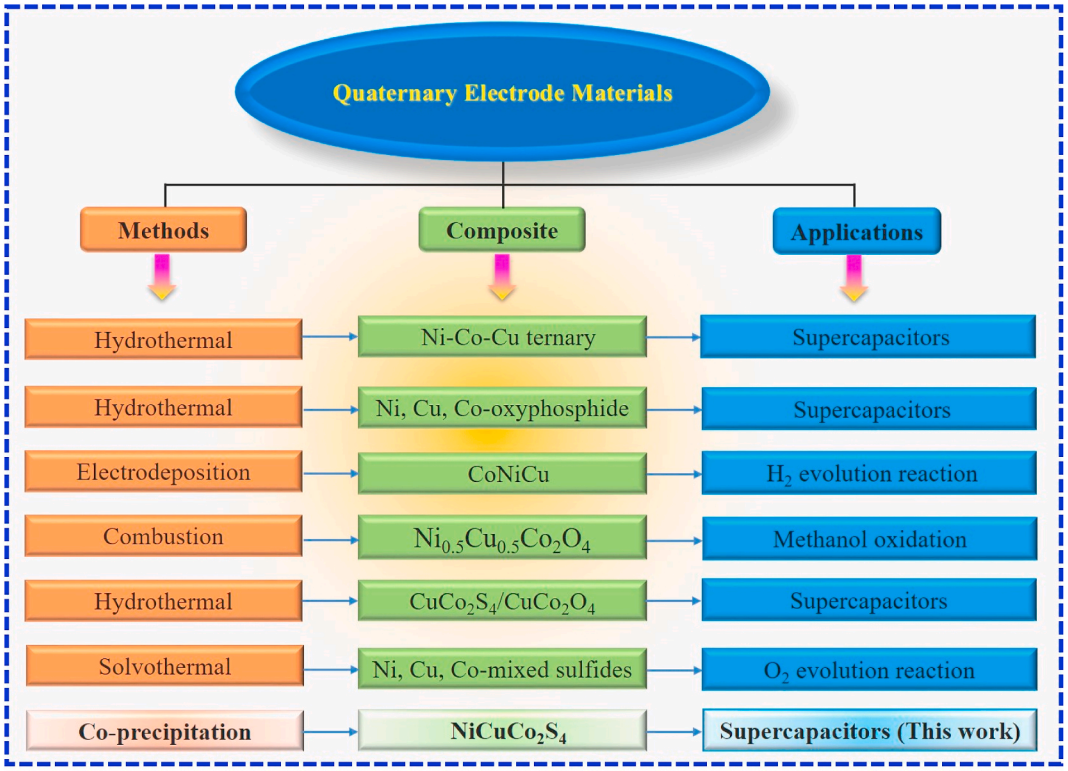

2. Experimental details

2.1. Materials

Analytical grade nickel (II) sulfate hexahydrate ($Ni(SO_4)\cdot 6H_2O$), cobalt(II) sulfate ($CoSO_4\cdot 7H_2O$), copper(II) sulfate $CuSO_4\cdot 2H_2O$, and sodium sulfide $Na_2S\cdot 9H_2O$ were procured from Sigma Aldrich.

2.2. Synthesis of $NiCuCo_2S_4$ by Co-precipitation method

To prepare the quaternary nanoflower-like $NiCuCo_2S_4$ nanocomposite, 0.2 g $NiSO_4\cdot 6H_2O$, 0.4 g $CoSO_4\cdot 7H_2O$, 0.4 g $CuSO_4\cdot 2H_2O$, and 0.4 g $Na_2S\cdot 9H_2O$ were mixed in 20 mL of double distilled water in separate vessels under constant stirring to obtain clear solutions. Ammonia solution added slowly into Ni, Cu, and Co solutions and pH was maintained to 11. After this, the Ni, Cu, and Co solutions were mixed thoroughly and 20 mL Na_2S added into it dropwise under constant stirring. Upon adding the sodium sulfide, a black precipitate formed within second, which indicates that the reaction was very fast. This mixture continuously stirred for 30 min and then the precipitate solution was filtered by Whatman paper and cleaned with distilled water. The synthesized $NiCuCo_2S_4$ powder was annealed at 300 °C for 1 h under an Argon atmosphere and its structure, morphology, and composition compared with the as-prepared composite. The annealed $NiCuCo_2S_4$ powder was used for further analysis. The screen-printing method employed in this study has been described elsewhere [31–33].

2.3. Characterization

XRD (XRD, Bruker D8 Advanced) analysis was used to study the structural properties of as prepared samples. A FE-SEM (FE-SEM; JEOL JSM-7100) and TEM (HR-TEM; JEOL JEM-2100) was employed to explore the surface morphology of the material. A Raman spectrometer (Jobin-Yvon LabRam-HR) and a XPS (XPS; ULVAC-PHI Quantera SXM) was utilized for structural and compositional analysis. The surface functional analysis of the materials was observed by a FT-IR (FT-IR, Nicolet 6700).

2.4. Electrochemical measurements

The electrochemical measurements such as CV, GCD, and EIS were performed on a Versa STAT 3 with a classical 3-electrode system in a 3 M KOH electrolyte. 0.15 mg/cm^2 of material coated on Ni foam used as working electrode. Pt and Ag/AgCl served as the counter and reference electrode, respectively.

2.5. Flexible solid-state hybrid (SHS) supercapacitor

A SHS device containing a polymer gel consisting of PVA and KOH was fabricated as reported previously [34,35]. The negative and positive electrodes were commercial AC and $NiCuCo_2S_4$, respectively; which separated by placing a piece of printing paper. The specific capacity (Cs), specific energy and power density was determined by the following formulae [34,35]:

$$C_s\left(mAhg^{-1}\right) = \frac{\int I(V)dv}{mv \times 3.6} \quad [1]$$

$$C_s\left(Cg^{-1}\right) = \frac{\int I(v)dv}{mV} \quad [2]$$

$$C_s\left(mAhg^{-1}\right) = \frac{I\int vdt}{mV} \quad [3]$$

$$\text{Specific energy density (ED)} = \frac{1}{2 \times 3.6} C_s V^2 \quad [4]$$

$$\text{Specific power density} = \frac{\text{ED} \times 3600}{T_d} \quad [5]$$

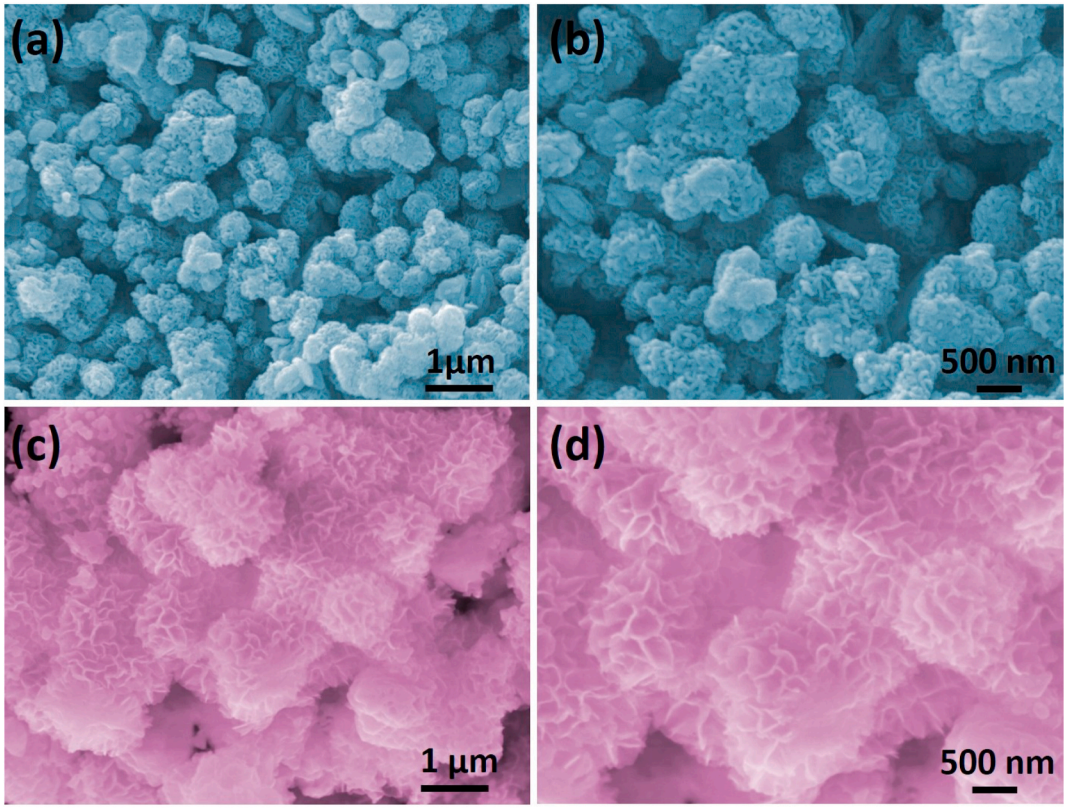

Fig. 1. (a–d) SEM images of the as-prepared and annealed $NiCuCo_2S_4$ at different magnifications.

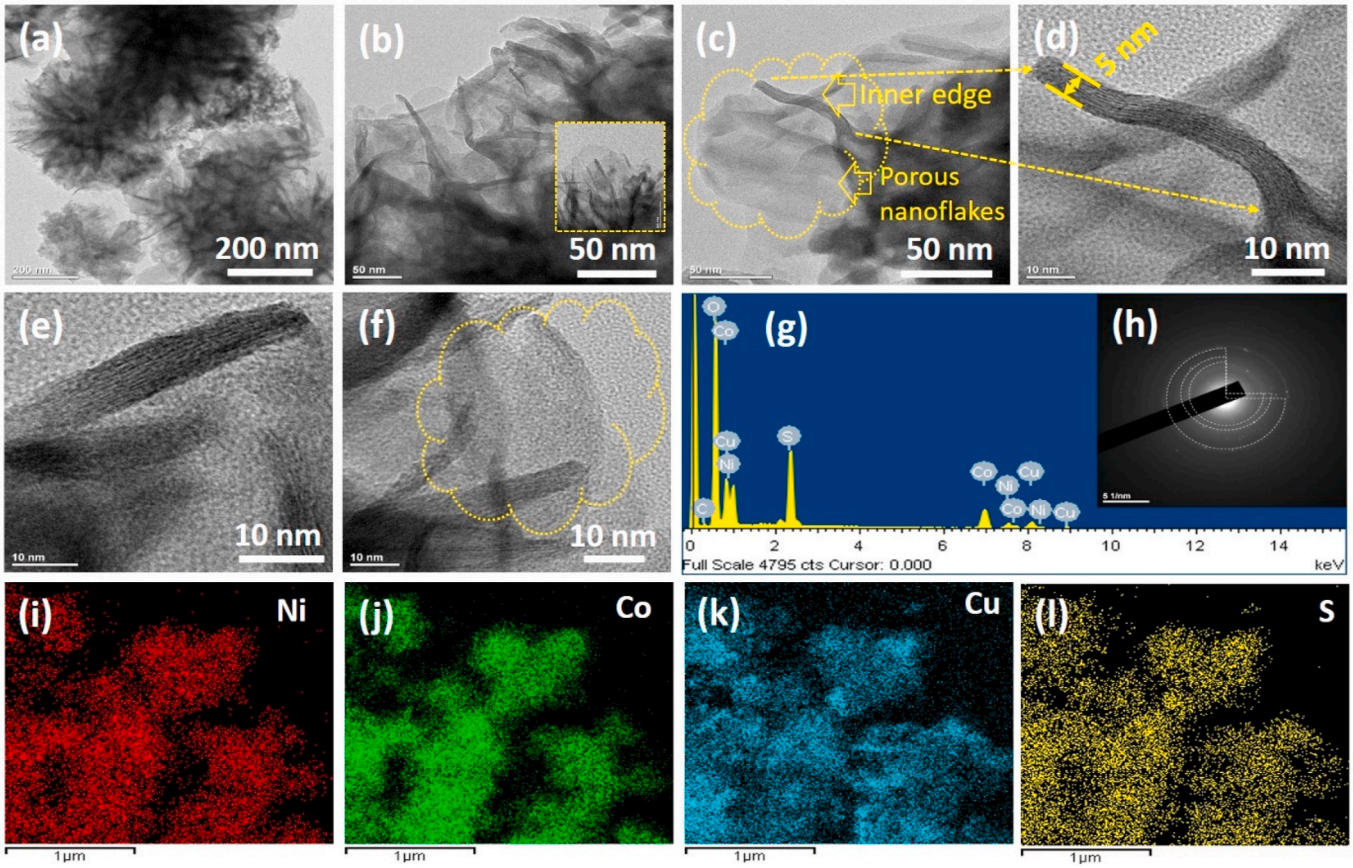

Fig. 2. (a–f) TEM images with different magnifications, (g) EDS, inset shows the SEAD pattern (h), and (i–l) elemental mapping of the optimized $NiCuCo_2S_4$.

3. Results and discussion

3.1. Surface morphological analysis

The effect of annealing on the $NiCuCo_2S_4$ composite was investigated by FE-SEM. Fig. 1(a–d) presents FE-SEM images of the as-prepared and annealed $NiCuCo_2S_4$ samples at different magnifications, respectively. Fig. 1(a, b) shows that uniform nanoflakes were present on the surface of the ternary $NiCuCo_2S_4$ samples before annealing. The morphological changes on the surface of the annealed $NiCuCo_2S_4$ samples are shown in Fig. 1(c, d). Highly porous nanoflower-like nanostructures with diameters of 500–600 nm have been reported to be uniformly present on the surface of ternary $NiCuCo_2S_4$ [36,37]. High-magnification images of the annealed $NiCuCo_2S_4$ in the present study revealed a similarly highly porous 3D nanoflower-like structure with numerous individually interconnected nanoflakes (5–10 nm) on the surface. This mesoporous nanoflake structure of the annealed $NiCuCo_2S_4$ is important for ion and electron transformation because this behavior of nanomaterials leads to a higher surface area [38]. The FE-SEM results show that the surface morphology of the annealed $NiCuCo_2S_4$ provided a greater active surface area, therefore it was used for further experimental analysis.

To evaluate the surface morphology and porosity of the annealed $NiCuCo_2S_4$ composite in more detail, the TEM analysis was also performed (Fig. 2a–f). The lower magnification images clearly show a uniform distribution of typical flower-like nanostructures on the surface of the $NiCuCo_2S_4$ composite, thus supporting the FE-SEM results. The higher magnification images revealed ultrathin, interconnected nanoflakes and highly transparent and porous nanowire-like dark and white lines (Fig. 2d, e). The thickness and length of the nanosheet were measured to be around 5–6 nm and 50–60 nm, respectively. The ultrathin edges and highly porous nanoflakes thus suggested that the $NiCuCo_2S_4$ composite would be useful for the transportation and transformation of ions and electrons [39,40]. The SAED patterns confirms the cubic polycrystalline nature of the sample of optimized $NiCuCo_2S_4$ [41–43]. EDS results proved the presence of Ni, Cu, Co, and S elements (Fig. 2g), confirming the successful formation of the $NiCuCo_2S_4$ composite. Elemental mapping images presented in Fig. 2(i–l) further confirms a homogeneous scattering of Ni, Cu, Co, and S on the surface of the $NiCuCo_2S_4$ composite. Overall, the EDS and elemental mapping analysis verify the formation of pure $NiCuCo_2S_4$.

3.2. X-ray diffraction analysis

The crystallography of the $NiCuCo_2S_4$ composite was studied by XRD technique. Fig. 3a present XRD patterns of the $NiCuCo_2S_4$ measured in the range of 20–80°. The characteristic peaks were detected at 2θ of 26.38°, 30.54°, 38.71°, 48.80°, 51.66°, 58.15°, 61.54°, 66.10°, and 76.02°, corresponding to the diffraction planes of (220), (311), (400), (422), (511), (531), (620), (533), and (642), respectively, for $NiCo_2S_4$ with a cubic crystal structure (JCPDS card:020–0782) (Fig. 3a) [44]. The remaining characteristic peaks were observed at 26.38°, 30.54°, 38.71°, 48.80°, 51.66°, 58.15°, 61.54°, and 76.02°, representing the cubic phase of the $CuCo_2S_4$, in particular the diffraction planes (220), (113), (004), (224), (115), (135), (026) and (137), respectively and matches with the standard JCPDS card 042–1450 (Fig. 3a). The XRD patterns illustrate the presence of both $NiCo_2S_4$ and $CuCo_2S_4$ and thus the formation of hybrid phases in the quaternary $NiCuCo_2S_4$ composite [45,46]. The XRD patterns of $NiCuCo_2S_4$ showed diffraction peaks at 26.38°, 30.54°, 38.71°, 48.80°, 58.15°, and 76.02° are ascribed to the (220), (311), (400), (511), (531), and (731) crystal planes of quaternary $NiCuCo_2S_4$ with a cubic crystal structure, confirming the formation of a pure quaternary $NiCuCo_2S_4$ composite (JCPDS card 029–0540). The increased peak intensity

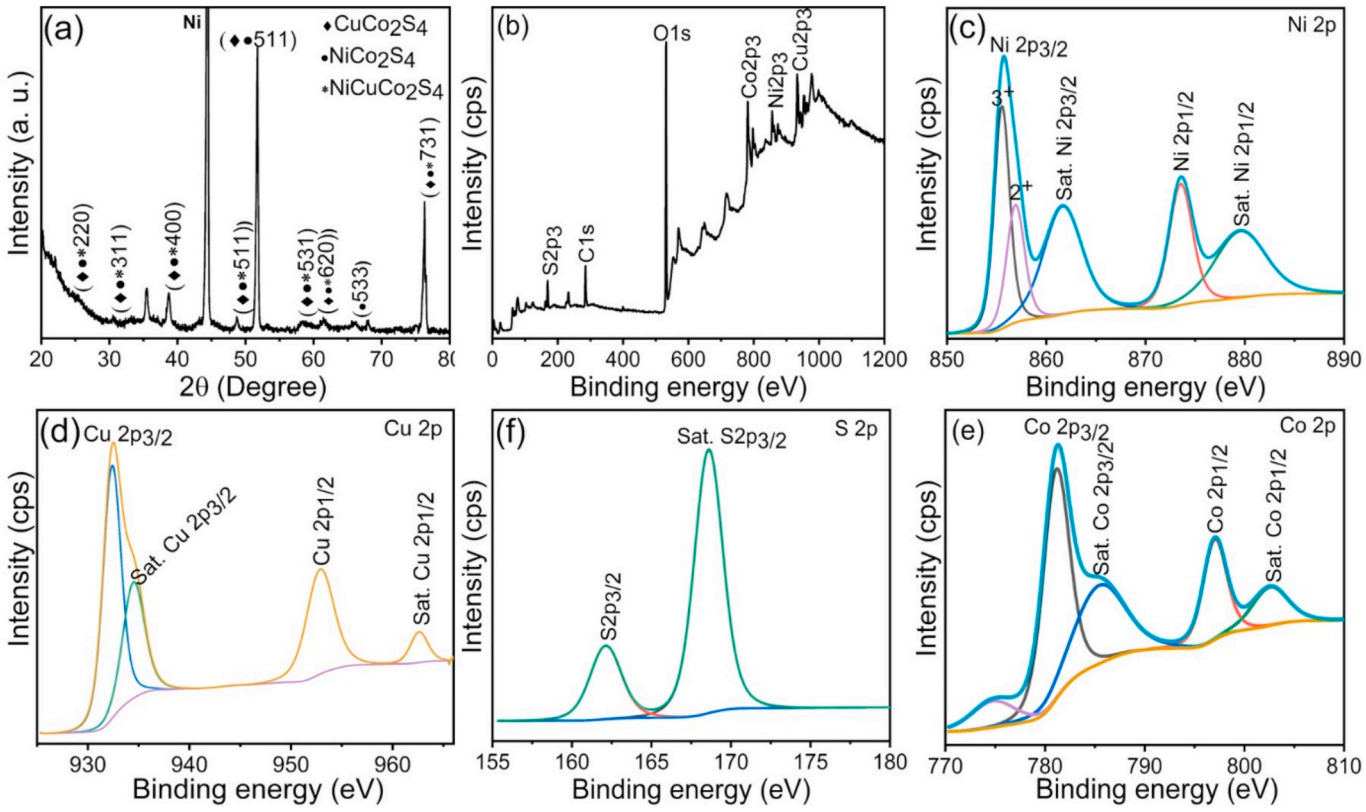

Fig. 3. (a) XRD pattern, (b) XPS survey spectra, (c) core levels of Ni 2p, (d) core levels of Cu 2p, (e) core levels of Co 2p, and (f) core levels of S 2p for the optimized $NiCuCo_2S_4$.

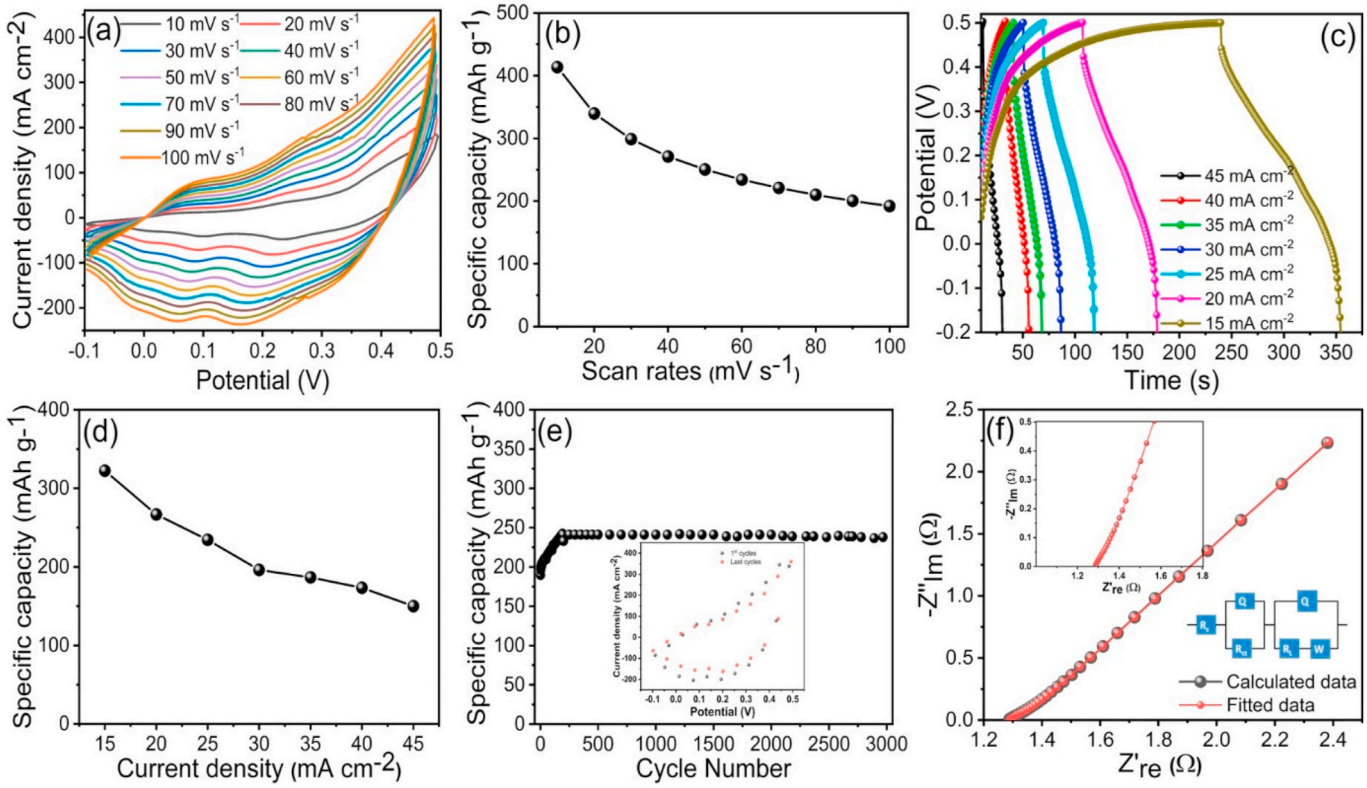

Fig. 4. (a) CV curves, (b) specific capacitance with respect to the scan rate, (c) GCD curves, (d) specific capacitance with respect to the current density, (e) cycling stability at 3000 cycles, and (f) Nyquist plots for the optimized $NiCuCo_2S_4$.

suggests the creation of more crystalline hybrid phases of $NiCo_2S_4$ and $CuCo_2S_4$ [46]. The obtained results also indicate the formation of pure phase $NiCuCo_2S_4$ [47]. No additional peaks were observed corresponding to other binary and ternary metal oxide or metal sulfide phases [48].

3.3. X-ray photoelectron spectroscopic analysis

The chemical constituents and elemental valence state of the prepared $NiCuCo_2S_4$ composite were studied by XPS. Fig. 3b presents the survey scan for the $NiCuCo_2S_4$ powder, revealing the presence of Ni, Cu, Co, and S. This also confirms the formation of quaternary $NiCuCo_2S_4$ compounds. The high-resolution spectrum of Ni is presented in Fig. 3c. Two major characteristic peaks for Ni 2p were appeared at 855.71 and 873.55 eV, corresponding to the Ni $2p_{3/2}$ and Ni $2p_{1/2}$ valence states [36,49]. The binding energy difference (ΔE) between these two electron configurations was around 17.84 eV, indicating the presence of both Ni^{3+} and Ni^{2+} species in the prepared $NiCuCo_2S_4$ [36,49,50]. Fig. 3d presents the high-resolution spectra of the Cu 2p spin-orbit valances, which show four dominant peaks. The characteristic peaks at 932.57 and 952.92 eV corresponded to the doublets of Cu $2p_{3/2}$ and Cu $2p_{1/2}$, respectively [41–43,48]. Satellite peaks of Cu $2p_{3/2}$ and Cu $2p_{1/2}$ were observed at 934.54 and 962.64 eV, respectively. The ΔE of Cu $2p_{3/2}$ and Cu $2p_{1/2}$ is about 20.35 eV, indicating the presence of Cu^{2+} species in the fabricated $NiCuCo_2S_4$ composite [46]. The high-resolution spectra for Co 2p shown in Fig. 3e revealed two intense peaks and two satellite peaks. The peaks at 781.22 and 797.05 eV were assigned to Co $2p_{3/2}$ and Co $2p_{1/2}$, respectively. The ΔE of Co $2p_{3/2}$ and Co $2p_{1/2}$ is 15.83 eV, suggesting the existence of both Co^{2+} and Co^{3+}. The satellite peaks were appeared at 785.82 and 802.84 eV, corresponding to Co $2p_{3/2}$ and Co $2p_{1/2}$, respectively (Fig. 3e) [45,46,51]. Fig. 3f presents the high-resolution for S2p, indicating the presence of S^{2-} in the prepared composite. The most intense peak was observed at 168.59 eV, representing the interaction of S^{2-} with the surface of the $NiCuCo_2S_4$ composite as sulfate or sulfite. Therefore, the XPS results confirmed the existence of Ni 2p, Cu 2p, Co 2p, and S 2p and thus the formation of quaternary $NiCuCo_2S_4$.

3.4. Electrochemical analysis

The supercapacitor properties of the optimized $NiCuCo_2S_4$/Ni electrode, as indicated by CV, GCD, and EIS measurements, were tested in a three-electrode system. Fig. 4a shows CV measurements for the $NiCuCo_2S_4$/Ni electrode at scan rates range from 10–100 mV s^{-1} with a potential range of −0.1 to 0.5 V. The redox reaction of $NiCuCo_2S_4$/Ni electrode and the KOH electrolyte resulted to strong reduction and oxidation peaks during the electrochemical testing [52,53]. As expected, the surface morphology of the $NiCuCo_2S_4$/Ni electrode provided a higher active surface area, increasing its Cs. The oxidation and reduction peaks in the CV shifted positively and negatively, respectively with an increase in the scan rates [53–56]. Fig. 4b presents the calculated Cs for scan rates of 10–100 mV s^{-1}. The Cs was 414, 339, 298, 270, 250, 234, 221, 209, 200 and 191 mAh g^{-1} at scan rates of 10–100 mV s^{-1}, respectively. These values are higher compared to the previously described values of ternary metal sulfide (Table 1), though very few reports are available on quaternary $NiCuCo_2S_4$.

Fig. 4c presents the GCD curves for the optimized $NiCuCo_2S_4$ electrode for current densities from 15-45 mA cm^{-2} with a potential range of −0.2 to 0.5 V. The CV curves show that the IR drop is much lower at 15 mA cm^{-2}, indicating higher Cs and strong Faradaic redox reactions of the $NiCuCo_2S_4$ electrode [57]. GCD curves illustrates the battery-like nature of the $NiCuCo_2S_4$ electrode. The charging and discharging nature of GCD curves were quite symmetrical, which indicates that the $NiCuCo_2S_4$ electrode had a higher cycling stability and coulombic efficiency [58]. Fig. 4d presents the Cs of the $NiCuCo_2S_4$ electrode for current densities of 15–45 mA cm^{-2}. The optimized $NiCuCo_2S_4$ electrode exhibited a Cs of 321, 266, 234, 196, 186, 173, and 150 mAh g^{-1} for the various current densities. The decrease in Cs values with an increase in the current density indicates that the prepared $NiCuCo_2S_4$ electrode was more stable and offered good stability and reversibility [53,59]. Interestingly, the Cs for the $NiCuCo_2S_4$ electrode in the existing analysis is higher than the previously described report (Table 1). The higher Cs of the $NiCuCo_2S_4$ electrode is attributed to the highly porous and ultrathin 3D nanoflakes nature which provides a higher active surface area [60].

The most important parameter in supercapacitor applications is stability, thus we investigated the cycling stability of the proposed electrode up to 3000 GCD cycles at 100 mV s^{-1} (Fig. 4e). The Cs increased for 300 cycles and then remained constant until 3000 cycles, with a capacity retention of 96%, representing higher stability [53,61,62]. These results indicated the suitability of the $NiCuCo_2S_4$ electrode towards the fabrication of a practical device. To understand the relationship between the prepared $NiCuCo_2S_4$ electrode and electrode, we performed EIS testing at 0.1 Hz–100 kHz in a KOH electrolyte (Fig. 4f). The sum of the solution ($R_s = 1.28\ \Omega$) and charge transfer resistance ($R_{ct} = 0.06\ \Omega$) for the $NiCuCo_2S_4$ electrode was low, indicating that the proposed electrode offers higher electrical conductivity and faster ion/electron transport from one layer to another [53,61–63].

After optimizing the $NiCuCo_2S_4$ as a possible active electrode material in supercapacitor using the 3-electrode approach, we constructed a two-electrode approach for a flexible SHS that utilized $NiCuCo_2S_4$ as the positive and AC as the negative electrodes, respectively. Fig. 5a presents the optimization of the potential range at various potentials with a constant scan rate. The CV show that the potential range increased from 1 to 1.9 V, while the current also increased from 22 to 44 mA cm^{-2}. Similar results were observed for the specific capacitance (Cs)

Table 1
Comparative study of $NiCuCo_2S_4$ materials and other composites.

Compounds	Specific capacity (mAh g^{-1})	Scan rates (mVs^{-1})	Current Density (A g^{-1})	Capability (%)	Potential (V)	Conc. of KOH Electrolyte (M)	Ref.
$NiCo_2S_4$	224	10	–	95	−0.1–0.6	1	5
$MnCo_2S_4$/HNTs	359	5	–	95	−02–0.5	1	15
$NiCo_2S_4$@$CoMoO_4$	353	–	1	88	0–0.6	2	16
Ni–Zn– $Co(CO_3)_{0.5}$ OH	280	–	1	80	0–0.5	3	20
$Zn_{0.6}Ni_{0.8}Co_{1.6}O_4$	347	–	1	88	−0.1–0.5	6	21
$NiCo_2O_4$/$NiCo_2S_4$	382	5	–	91	−0.2–0.5	2	26
$NiCo_2O_4$/$NiCo_2O_4$	322	5	–	94	−0.1–0.5	3	27
rGO- $NiCo_2O_4$	161	–	0.5	76	−0.1–0.5	3	28
$CuCo_2S_4$/$CuCo_2O_4$	166	–	1	85	0–0.5	2	43
$NiCo_2S_4$@$CoMoO_4$	353	–	1	86	0–0.6	2	47
Ni–Mn–S@$NiCo_2S4$	260	–	1	79	0–0.6	2	49
$NiCo_2S4$	208	–	3	–	−0.1–0.4	2	50
$NiCuCo_2S_4$	*414*	*10*	-	*96*	*−0.1–0.5*	*3*	*This work*

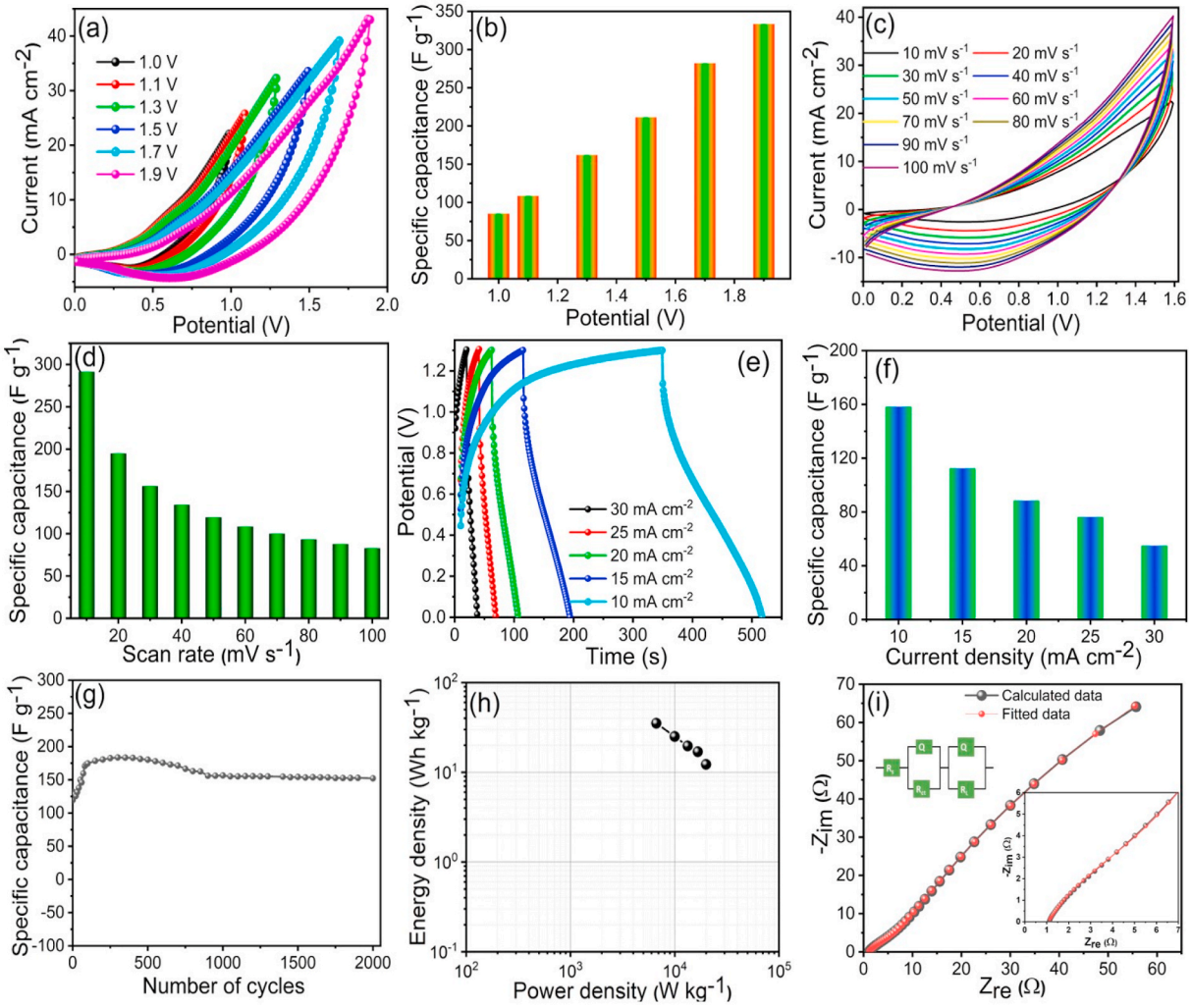

Fig. 5. (a, b) Potential windows in relation to the specific capacitance, (c) CV curves at the optimized potential window of 1.6 V with respect to the scan rate (10–100 mV s^{-1}), (d) specific capacitance vs scan rate, (e) GCD curves with respect to the current density (10–30 mA cm^{-2}), (f) specific capacitance vs current density, (g) cycling stability, (h) Ragone plots, and (i) Nyquist plots for the solid-state $NiCuCo_2S_4$//AC ASC.

with respect to the potential as shown in Fig. 5b. A 1.6 V window was considered most suitable for further electrochemical analysis because a higher area was observed in the CV curves (Fig. 5b). Fig. 5c presents the CV measurements for the SHS of $NiCuCo_2S_4$//AC at a different scan rate. The higher Cs value was obtained of about 290 F g^{-1} with a scan rate of 10 mV s^{-1} (Fig. 5d) compared to the previously reported ternary materials.

To our knowledge, this is the first study on a quaternary $NiCuCo_2S_4$ electrode for a SHS device. The $NiCuCo_2S_4$ electrode exhibited a higher electrochemical performance because the 3D nanoflower-like nanostructure provided a higher surface area, the highly porous surface allowed more rapid transportation of electrons and ions, and reversible and rapid Faradaic reactions were possible [63]. Fig. 5e displays the GCD curves for the $NiCuCo_2S_4$//AC SHS at current densities from 10 to 30 mA cm^{-2}, with a potential window 0–1.3 V. The GCD curves exhibited similar behavior, illustrating the outstanding reversibility of the $NiCuCo_2S_4$//AC hybrid device [63]. Fig. 5f presents the obtained Cs with respect to the various current densities. The Cs decreased from the 159 to 56 F g^{-1} with an increase in current density from 10 to 30 mA cm^{-2}, respectively. This indicated higher long-term stability of the $NiCuCo_2S_4$//AC device [64]. To confirm this, we conducted cycling stability tests and the results are shown in Fig. 5g. The $NiCuCo_2S_4$//AC hybrid device demonstrated a constant cycling stability of 94.3% up to 2000 cycles, proving that the fabricated $NiCuCo_2S_4$//AC SHS device has a suitable high capacity [62–64]. The most important parameter in the application of SHS devices is its energy and power density. The results for the fabricated $NiCuCo_2S_4$//AC hybrid device are presented as a Ragone plot in Fig. 5h. The specific energy was about 35.19 Wh kg^{-1} and the specific power was about 0.66 kWh g^{-1} at a low current density of 10 mA cm^{-2}, while the specific energy was about 12.21 Wh kg^{-1} and the specific power was about 20 kWh g^{-1} at a high current density of 30 mA cm^{-2}, indicating that the $NiCuCo_2S_4$//AC SHS device was highly stable [64,65]. The calculated values of the specific energy and power density in the existing analysis's are higher than previously described studies, for instance NCS@NCS//RGO (24.9 Wh kg^{-1} at 334 W kg^{-1}) [66], CuCoO–H (32.2 Wh kg^{-1} at 644 W kg^{-1}) [67], $NiCo_2S_4$ [21.8 Wh kg^{-1} at 14 kW kg^{-1}] [68], and $NiCo_2S_4$ [28.3 Wh Kg^{-1} at 245 W kg^{-1}] [69]. Nyquist plots for the $NiCuCo_2S_4$//AC device are shown in Fig. 5i. The R_s and R_{ct} of the ASC device was about 1.07 Ω and 4.44 Ω, respectively. The sum of R_s and R_{ct} was low, which indicates that the $NiCuCo_2S_4$//AC hybrid device exhibited an excellent electrical properties and is suitable for practical applications.

4. Conclusions

The fabrication approach demonstrated in the present study effectively enhanced the properties of the quaternary nanoflower-like $NiCuCo_2S_4$ electrode. The highly porous 3D nanoflower-like

$NiCuCo_2S_4$ electrode provided a high surface area, which is useful for improving supercapacitive performance. The morphological results confirmed that annealing improved the supercapacitive performance of the quaternary $NiCuCo_2S_4$. The porous nanoflower-like $NiCuCo_2S_4$ electrode displayed a high Cs of 414 mAh g^{-1} at 10 mV s^{-1} with good cycling capacities. Furthermore, the fabricated $NiCuCo_2S_4$//AC SHS device offered an advanced energy and power density of 35.19 Wh kg^{-1} and 0.66 kW kg^{-1}, respectively. Thus, present results confirmed that we effectively established a strategy for the fabrication of a quaternary TMS of a novel $NiCuCo_2S_4$ electrode with enhanced structural, morphological, and electrochemical characteristics.

Declaration of competing interest

The authors declare that they have no known competing financial interests or personal relationships that could have appeared to influence the work reported in this paper.

Acknowledgement

Analysis of samples was supported by Dongguk University, Seoul, Korea Research Fund 2020–2022.

ADJ is thankful to the Department of Science and Technology (DST), Govt. of India for financial assistance under the DST INSPIRE Faculty Scheme [DST/INSPIRE/04/2017/002737].

References

[1] C. Zhang, H. Yin, M. Han, Z. Dai, H. Pang, Y. Zheng, Y.Q. Lan, J. Bao, J. Zhu, Two-dimensional tin selenide nanostructures for flexible all-solid-state supercapacitors, ACS Nano 8 (2014) 3761–3770.

[2] P.J. Hall, E.J. Bain, Energy-storage technologies and electricity generation, Energy Pol. 36 (2008) 4352–4355.

[3] H.M. Yadav, N.C.D. Nath, J. Kim, S.K. Shinde, S. Ramesh, F. Hossain, O. Ibukun, J. J. Lee, Nickel-Graphene nanoplatelet deposited on carbon fiber as binder-free electrode for electrochemical supercapacitor application, Polymers 12 (2020) 1666.

[4] S.K. Shinde, G.S. Ghodake, D.P. Dubal, H.D. Dhaygude, D.-Y. Kim, V.J. Fulari, Enhanced photoelectrochemical properties of nanoflower-like hexagonal $CdSe_{0.6}Te_{0.4}$:Effect of electron beam irradiation, J. Ind. Eng. Chem. 45 (2017) 92–98.

[5] D.-Y. Kim, G.S. Ghodake, N.C. Maile, A.A. Kadam, Lee Sung, V.J. Fulari, S. K. Shinde, Chemical synthesis of hierarchical $NiCo_2S_4$ nanosheets like nanostructure on flexible foil for a high performance supercapacitor, Sci. Rep. 7 (2017) 9764.

[6] T. Deng, W. Zhang, O. Arcelus, J.G. Kim, J. Carrasco, S.J. Yoo, W. Zheng, J. Wang, H. Tian, H. Zhang, X. Cui, T. Rojo, Atomic-level energy storage mechanism of cobalt hydroxide electrode for pseudocapacitors, Nat. Commun. 8 (2017) 1–9.

[7] G. Wang, L. Zhang, J. Zhang, A review of electrode materials for electrochemical supercapacitors, Chem. Soc. Rev. 41 (2012) 797–828.

[8] H. Chen, S. Chen, M. Fan, C. Li, D. Chen, G. Tian, K. Shu, Bimetallic nickel cobalt selenides: a new kind of electroactive material for high-power energy storage, J. Mater. Chem. A 3 (2015) 23653–23659.

[9] B. Chen, Y. Tian, Z. Yang, Y. Ruan, J. Jiang, C. Wang, Construction of (Ni, Cu) Se_2//reduced graphene oxide for high energy density asymmetric supercapacitor, ChemElectroChem 4 (2017) 3004–3010.

[10] Q. Sun, H. Cheng, X. Mei, Y. Liu, G. Li, Q. Xu, X. Lu, Efficient synchronous extraction of nickel, copper, and cobalt from low–nickel Matte by sulfation roasting–water leaching process, Sci. Rep. 10 (2020) 9916.

[11] T.S. Mathis, N. Kurra, X. Wang, D. Pinto, P. Simon, Y. Gogotsi, Energy storage data reporting in perspective-guidelines for interpreting the performance of electrochemical energy storage systems, Adv. Energy Mater. 9 (2019) 1902007.

[12] P. Simon, Y. Gogotsi, B. Dunn, Where do batteries end and supercapacitors begin? Science 343 (2014) 1210–1211.

[13] Y. Ge, J. Wu, X. Xu, M. Ye, J. Shen, Facile synthesis of $CoNi_2S_4$ and $CuCo_2S_4$ with different morphologies as prominent catalysts for hydrogen evolution reaction, Int. J. Hydrogen Energy 41 (2016) 19847–19854.

[14] X. Wu, S. Li, B. Wang, J. Liu, M. Yu, $NiCo_2S_4$ nanotube arrays grown on flexible nitrogen-doped carbon foams as three-dimensional binder-free integrated anodes for high-performance lithium-ion batteries, Phys. Chem. Chem. Phys. 18 (2016) 4505–4512.

[15] S.K. Shinde, G.S. Ghodake, N.C. Maile, H.M. Yadav, A.D. Jagadale, M.B. Jalak, A. A. Kadam, S. Ramesh, C. Bathula, D.-Y. Kim, Designing of nanoflakes anchored nanotubes-like $MnCo_2S_4$/halloysite composites for advanced battery like supercapacitor application, Electrochim. Acta 341 (2020), 135973.

[16] Y. Zhao, X. He, R. Chen, Q. Liu, J. Liu, D. Song, H. Zhang, H. Dong, R. Li, M. Zhang, J. Wang, Hierarchical $NiCo_2S_4$@$CoMoO_4$ core-shell heterostructures nanowire arrays as advanced electrodes for flexible all-solid-state asymmetric supercapacitors, Appl. Surf. Sci. 453 (2018) 73–82.

[17] J. Long, Z. Hou, C. Shu, C. Han, W. Li, R. Huang, J. Wang, Free-Standing three-dimensional $CuCo_2S_4$ nanosheet array with high catalytic activity as an efficient oxygen electrode for lithium-oxygen batteries, ACS Appl. Mater. Interfaces 11 (2019) 3834–3842.

[18] L. Xu, L. Zhang, B. Cheng, J. Yu, A.A. Al-Ghamdi, S. Wageh, Significant capacitance enhancement induced by cyclic voltammetry in pine needle-like Ni-Co- Cu multicomponent electrode, J. Mater. Sci. Technol. 78 (2020) 100–109.

[19] X. Wu, S. Li, J. Liu, M. Yu, Multiplex compounds of Ni, Cu, Co-based oxyphosphide nanowire arrays grown on Ni foam: a well-designed free-standing anode for high-capacity lithium storage, J. Alloys Compd. 799 (2019) 406–414.

[20] H. Gu, Q. Zhong, Y. Zeng, S. Zhang, Y. Bu, Ni and Zn co-substituted $Co(CO_3)_{0.5}OH$ self-assembled flowers array for asymmetric supercapacitors, J. Colloid Interface Sci. 573 (2020) 299–306.

[21] M.T. Ahsan, M. Usman, Z. Ali, S. Javed, R. Ali, M.U. Farooq, M.A. Akram, A. Mahmood, A 3D hierarchically mesoporous zinc-nickel-cobalt ternary oxide ($Zn_{0.6}Ni_{0.8}Co_{1.6}O_4$) nanowires for high-performance asymmetric supercapacitors, Front. Chem. 8 (2020) 487.

[22] A. Karpuz, H. Kockar, M. Alper, Study of electrolyte pH in production of Cu-Co-Ni ternary alloys and its effect on microstructural and magnetic properties, IEEE Trans. Magn. 50 (2014).

[23] K.N. Ignatova, Y.S. Marcheva, Electrodeposition and structure of Co coatings (CoCu, NiCo and CoNiCu) in potentiostatic and pulse potential modes, Bulg. Chem. Commun. 45 (2013) 57–63.

[24] M. Jafarian, T. Rostami, M.G. Mahjani, F.A. Gobal, A low cost and highly active non-noble alloy electrocatalyst for hydrazine oxidation based on nickel ternary alloy at the surface of graphite electrode, J. Electroanal. Chem. 763 (2016) 134–140.

[25] L. Xu, L. Zhang, B. Cheng, J. Yu, A.A. Al-Ghamdi, S. Wageh, Significant capacitance enhancement induced by cyclic voltammetry in pine needle-like Ni-Co-Cu multicomponent electrode, J. Mater. Sci. Technol. 78 (2021) 100–109.

[26] X. Wu, S. Li, J. Liu, M. Yu, Multiplex compounds of Ni, Cu, Co-based oxyphosphide nanowire arrays grown on Ni foam: a well-designed free-standing anode for high-capacity lithium storage, J. Alloys Compd. 799 (2019) 406–414.

[27] C. Wang, W. Li, X. Lu, S. Xie, F. Xiao, P. Liu, Y. Tong, Facile synthesis of porous 3D CoNiCu nano-network structure and their activity towards hydrogen evolution reaction, Int. J. Hydrogen Energy 37 (2012) 18688–18693.

[28] S. Samanta, K. Bhunia, D. Pradhan, B. Satpati, R. Srivastava, $NiCuCo_2O_4$ supported Ni−Cu ion-exchanged mesoporous zeolite heteronano architecture: an efficient, stable, and economical nonprecious electrocatalyst for methanol oxidation, ACS Sustain. Chem. Eng. 6 (2018) 2023–2036.

[29] X. Xu, Y. Liu, P. Dong, P.M. Ajayan, J. Shen, M. Ye, Mesostructured $CuCo_2S_4$/$CuCo_2O_4$ nanoflowers as advanced electrodes for asymmetric supercapacitors, J. Power Sources 400 (2018) 96–103.

[30] X. Wu, S. Li, J. Liu, M. Yu, Mesoporous hollow nested nanospheres of Ni, Cu, Co-based mixed sulfides for electrocatalytic oxygen reduction and evolution, ACS Appl. Nano Mater. 2 (2019) 4921–4932.

[31] S.K. Shinde, G.S. Ghodake, N.C. Maile, H.M. Yadav, A.D. Jagadale, M.B. Jalak, A. A. Kadam, Sivalingam Ramesh, C. Bathula, D.-Y. Kim, Designing of nanoflakes anchored nanotubes-like $MnCo_2S_4$/halloysite composites for advanced battery like supercapacitor application, Electrochim. Acta 341 (2020), 135973.

[32] S.K. Shinde, M.B. Jalak, G.S. Ghodake, N.C. Maile, H.M. Yadav, A.D. Jagadale, Asif Shahzad, D.S. Lee, A.A. Kadam, V.J. Fulari, D.-Y. Kim, Flower-like $NiCo_2O_4$/$NiCo_2S_4$ electrodes on Ni mesh for higher supercapacitor applications, Ceram. Int. 45 (2019) 17192–17203.

[33] S.K. Shinde, H.M. Yadav, S. Ramesh, C. Bathula, N. Maile, G.S. Ghodake, H. Dhaygude, D.-Y. Kim, High-performance symmetric supercapacitor; nanoflower-like $NiCo_2O_4$//$NiCo_2O_4$ thin films synthesized by simple and highly stable chemical method, J. Mol. Liquids 299 (2020), 112119.

[34] A. Mondal, S. Maiti, S. Mahanty, A.B. Pand, Large-scale synthesis of porous $NiCo_2O_4$ and rGO-$NiCo_2O_4$ hollowspheres with superior electrochemical performance as faradaic electrode, J. Mater. Chem. A 5 (2017) 16854–16864.

[35] A.M. Patil, X. An, S. Li, X. Yue, X. Du, A. Yoshida, X. Hao, A. Abudula, G. Guan, Fabrication of three-dimensionally heterostructured rGO/WO_3·$0.5H_2O$@Cu_2S electrodes for high-energy solid-state pouch-type asymmetric supercapacitor, Chem. Eng. J. 403 (2021), 126411.

[36] X. Wu, S. Li, J. Liu, M. Yu, Multiplex compounds of Ni, Cu, Co-based oxyphosphide nanowire arrays grown on Ni foam: a well-designed free-standing anode for high-capacity lithium storage, J. Alloys Compd. 799 (2019) 406–414.

[37] S.K. Shinde, S.M. Mohite, A.A. Kadam, H.M. Yadav, G.S. Ghodake, K.Y. Rajpure, D. S. Lee, D.-Y. Kim, Effect of deposition parameters on spray pyrolysis synthesized CuO nanoparticle thin films for higher supercapacitor performance, J. Electroanal. Chem. 850 (2019), 113433.

[38] S.K. Shinde, V.J. Fulari, D.-Y. Kim, N.C. Maile, R.R. Koli, H.D. Dhaygude, G. S. Ghodake, Chemical synthesis of flower-like hybrid $Cu(OH)_2$/CuO electrode: application of polyvinyl alcohol and triton X-100 to enhance supercapacitor performance, Colloids Surf., B 156 (2017) 165–174.

[39] J. Long, Z. Hou, C. Shu, C. Han, W. Li, R. Huang, J. Wang, Free-Standing three-dimensional $CuCo_2S_4$ nanosheet array with high catalytic activity as an efficient oxygen electrode for Lithium−Oxygen batteries, ACS Appl. Mater. Interfaces 11 (2019) 3834–3842.

[40] S. Shinde, H. Dhaygude, D.-Y. Kim, G. Ghodake, P. Bhagwat, P. Dandge, V. Fulari, Improved synthesis of copper oxide nanosheets and its application in development of supercapacitor and antimicrobial agents, J. Ind. Eng. Chem. 36 (2016) 116–120.

[41] S. Hao, B. Ouyang, C. Li, B. Zhang, J. Feng, J. Wu, M. Srinivasan, Y. Huang, Hollow mesoporous Co(PO3)2@Carbon polyhedra as high performance anode materials for lithium ion batteries, J. Phys. Chem. C 123 (2019) 8599–8606.
[42] S.K. Shinde, D.-Y. Kim, G.S. Ghodake, N.C. Maile, A.A. Kadam, D.S. Lee, M.C. Rath, V.J. Fulari, Morphological enhancement to CuO nanostructures by electron beam irradiation for biocompatibility and electrochemical performance, Ultrason. Sonochem. 40 (2018) 314–322.
[43] H.M. Yadav, G.S. Ghodake, D.-Y. Kim, Sivalingam Ramesh, N.C. Maile, D.S. Lee, S. K. Shinde, Nanorods to hexagonal nanosheets of CuO-doped manganese oxide nanostructures for higher electrochemical supercapacitor performance, Colloids Surf., B 184 (2019) 110500.
[44] X. Wu, S. Li, J. Liu, M. Yu, Mesoporous hollow nested nanospheres of Ni, Cu, Co-based mixed sulfides for electrocatalytic oxygen reduction and evolution, ACS Appl. Nano Mater. 2 (2019) 4921–4932.
[45] S. Samanta, K. Bhunia, D. Pradhan, B. Satpati, R. Srivastava NiCuCo2O4, Supported Ni−Cu ion-exchanged mesoporous zeolite heteronano architecture: an efficient, stable, and economical nonprecious electrocatalyst for methanol oxidation, ACS Sustain. Chem. Eng. 6 (2018) 2023–2036.
[46] D. Wang, X. Zhang, Z. Du, Z. Mo, Y. Wu, Q. Yang, Y. Zhang, Z. Wu, CoNi2S4 nanoparticles as highly efficient electrocatalysts for the hydrogen evolution reaction in alkaline media, Int. J. Hydrogen Energy 42 (2017) 3043–3050.
[47] A.R. Patel, G. Patel, G. Maity, S.P. Patel, S. Bhattacharya, A. Putta, S. Banerjee, Direct oxidative azo coupling of anilines using a self-assembled flower-like $CuCo_2O_4$ material as a catalyst under aerobic conditions, ACS Omega 5 (47) (2020) 30416–30424.
[48] X. Xu, Y. Liu, P. Dong, P.M.A.J. Shen, M. Ye, Mesostructured $CuCo_2S_4$/$CuCo_2O_4$ nanoflowers as advanced electrodes for asymmetric supercapacitors, J. Power Sources 400 (2018) 96–103.
[49] X. Wu, S. Li, B. Wang, J. Liu, M. Yu, Mesoporous Nisingle bondCo based nanowire arrays supported on three-dimensional N-doped carbon foams as non-noble catalysts for efficient oxygen reduction reaction, Microporous Mesoporous Mater. 231 (2016) 128–137.
[50] D. Cai, D. Wang, C. Wang, B. Liu, L. Wang, Y. Liu, Q. Li, T. Wang, Construction of desirable NiCo2S4 nanotube arrays on nickel foam substrate for pseudocapacitors with enhanced performance, Electrochim. Acta 151 (2015) 35–41.
[51] S. Czioska, J. Wang, X. Teng, Z. Chen, Hierarchically structured CuCo2S4 nanowire arrays as efficient bifunctional electrocatalyst for overall water splitting, ACS Sustain. Chem. Eng. 6 (2018) 11877–11883.
[52] S.K. Shinde, M.B. Jalak, S.Y. Kim, H.M. Yadav, G.S. Ghodake, A.A. Kadam, D.-Y. Kim, Effect of Mn doping on the chemical synthesis of interconnected nanoflakes-like CoS thin films for high performance supercapacitor applications, Ceram. Int. 44 (2018) 23102–23108.
[53] Y. Zhao, X. He, R. Chen, Q. Liu, J. Liu, D. Song, H. Zhang, H. Dong, R. Li, M. Zhang, J. Wang, Hierarchical $NiCo_2S_4$@$CoMoO_4$ core-shell heterostructures nanowire arrays as advanced electrodes for flexible all-solid-state asymmetric supercapacitors, Appl. Surf. Sci. 453 (2018) 73–82.
[54] S.K. Shinde, D.P. Dubal, G.S. Ghodake, D.Y. Kim, V.J. Fulari, Nanoflower-like CuO/Cu(OH)2 hybrid thin films: synthesis and electrochemical supercapacitive properties, J. Electroanal. Chem. 732 (2014) 80–85.
[55] L. Wan, Y. Yuan, J. Liu, J. Chen, Y. Zhang, C. Du, M. Xie, A free-standing Ni–Mn–S@NiCo2S4 core–shell heterostructure on carbon cloth for high-energy flexible supercapacitors, Electrochim. Acta 368 (2021), 137579.
[56] S. Sahoo, K.K. Naik, C.S. Rout, Controlled electrochemical growth of spinel NiCo2S4 nanosheets on nickel foam for high performance supercapacitor applications, Mater. Today: PRO 5 (2018), 23083–2308.
[57] S. Zhao, J. Xu, M. Mao, L. Li, X. Li, NiCo2S4@Zn0.5Cd0.5S with direct Z-scheme heterojunction constructed by band structure adjustment of ZnxCd1-xS for efficient photocatalytic H2 evolution, Appl. Surf. Sci. 528 (2020), 147016.
[58] Y. Yan, A. Li, C. Lu, T. Zhai, S. Lu, W. Li, W. Zhou, Double-layered yolk-shell microspheres with NiCo2S4-Ni9S8-C hetero-interfaces as advanced battery-type electrode for hybrid supercapacitors, Chem. Eng. J. 396 (2020), 125316.
[59] Z. Wang, L.C. Nengzi, X. Zhang, Z. Zhao, X. Cheng, Novel NiCo2S4/CS membranes as efficient catalysts for activating persulfate and its high activity for degradation of nimesulide, Chem. Eng. J. 381 (2020), 122517.
[60] H. Zhang, H. Li, Z. Sun, D. Ji, One-step hydrothermal synthesis of NiCo2S4 nanoplates/nitrogen-doped mesoporous carbon composites as advanced electrodes for asymmetric supercapacitors, J. Power Sources 439 (2019), 227082.
[61] Y. Cheng, M. Zhai, J. Hu, The fabrication of NiCu2S2 from NiCu film on nickel foam for methanol electrooxidation and supercapacitors, Appl. Surf. Sci. 480 (2019) 505–513.
[62] M. Dong, Z. Wang, G. Yan, J. Wang, H. Guo, X. Li, Confine growth of NiCo2S4 nanoneedles in graphene framework toward high-performance asymmetric capacitor, J. Alloys Compd. 822 (2020), 153645.
[63] R. Zhai, Y. Xiao, T. Ding, Y. Wu, S. Chen, W. Wei, Construction of NiCo2S4 heterostructure based on electrochemically exfoliated graphene for high-performance hybrid supercapacitor electrode, Journal of Alloy Compd 845 (2020), 156164.
[64] L. Kang, C. Huang, J. Zhang, M. Zhang, N. Zhang, S. Liu, Y. Ye, C. Luo, Z. Gong, C. Wang, X. Zhou, X. Wu, S.C. Jun, Effect of fluorine doping and sulfur vacancies of CuCo2S4 on its electrochemical performance in supercapacitors, Chem. Eng. J. 390 (2020), 124643.
[65] S.K. Shinde, M.B. Jalak, G.S. Ghodake, N.C. Maile, V.S. Kumbhar, D.S. Lee, V. J. Fulari, D.-Y. Kim, Chemically synthesized nanoflakes-like NiCo2S4 electrodes for high-performance supercapacitor application, Appl. Surf. Sci. 466 (2019) 822–829.
[66] H. Chen, S. Chen, H. Shao, C. Li, M. Fan, D. Chen, G. Tian, K. Shu, Hierarchical NiCo2S4 nanotube@ NiCo2S4 nanosheet arrays on Ni foam for high-performance supercapacitors, Chem. Asian J. 11 (2016) 248–255.
[67] C. Jin, Y. Cui, G. Zhang, W. Luo, Y. Liu, Y. Sun, Z. Tian, W. Zheng, Synthesis of copper-cobalt hybrid oxide microflowers as electrode material for supercapacitors, Chem. Eng. J. 343 (2018) 331–339.
[68] X. Xu, X. Tian, X. Li, T. Yang, Y. He, K. Wang, Y. Song, Z. Liu, Structural and chemical synergistic effect of NiCo2S4 nanoparticles and carbon cloth for high performance binder-free asymmetric supercapacitors, Appl. Surf. Sci. 465 (2019) 635–642.
[69] Y. Zhu, Z. Wu, M. Jing, X. Yang, W. Song, X. Ji, Mesoporous $NiCo_2S_4$ nanoparticles as high-performance electrode materials for supercapacitors, J. Power Sources 273 (2015) 584–590.